Advances in Geo-Energy Research

Vol. 5, No. 4, p. 465-472, 2021

Original article

Theoretical study of micropolar fluid flow in porous media

Weiyao Zhu*

School of Civil and Resources Engineering, University of Science and Technology Beijing, Beijing 100083, P. R. China

Keywords:
Micropolar fluid
unsteady radial flow
Hele-Shaw flow
non-Newtonian fluid

Cited as:
Zhu, W. Theoretical study of micropolar fluid flow in porous media. Advances in Geo-Energy Research, 2021, 5(4): 465-472, doi: 10.46690/ager.2021.04.11

Abstract:
In this paper, a mathematical model of Hele-Shaw flow was developed on the basis of the field equation of micropolar fluid. The motion equation of micropolar fluid was extended to flow in porous media, contributing to the mathematical model of the unsteady radial flow of micropolar fluid in an infinite reservoir. The relations between flow velocity, pressure gradient and flow rate were obtained by solving the mathematical model under fixed production internal boundary and fixed-pressure external boundary conditions. In addition, the effect of the physical properties of micropolar fluid on its flow was analyzed. The results indicated a significant dependence between the apparent permeability and physical properties of micropolar fluid, which clearly deviated from the Newtonian fluid. The results showed that, as the ratio of rotational viscous force to Newtonian viscous force in the micropolar parameter and the characteristic length of the micropolar metamaterial increase, the non-Newtonian characteristics of the fluid become gradually more significant. The non-Newtonian behavior of micropolar fluid consequently becomes unneglected, leading to a decreasing apparent permeability. Compared with a Newtonian fluid, a micropolar fluid causes obvious flow resistance, resulting in larger energy consumption and lower flow rate. This study can provide an academic reference for nonlinear rheology and the flow of heterogeneous fluids in the fields of petroleum engineering and biofluid flow.

1. Introduction

With the advance of the continuous flow field theory, the micropolar field theory has been applied to the study of matter with a certain internal structure. Studies on polymer fluids, the cooling of a metallic plate in a bath, animal bloods, exotic lubricants, and colloidal or suspension solutions are typical applications of this theory (Siddheshwar and Manjunath, 2000; Chang-Jian and Chen, 2006; Nabwey and Mahdy, 2021; Yadav and Kumar, 2021). According to numerous experiments, nonlinear rheological behaviors appear when heterogeneous fluids transport in a porous media or a narrow channel compared to fluid molecules (or particles included in fluid) with characteristic size (Chen and Price, 2006; Lok et al., 2007). For instance, the viscosity of blood measured in a porous media is larger than that measured in a conventional channel (Masuda et al., 1992; Ellahi et al., 2014; Mohamadian et al., 2018). Due to the poorer applicability of the classic theory, various non-Newtonian fluid models have been proposed to describe this phenomenon. The relationship between shear stress and shear strain rate of a non-Newtonian fluid shows a nonlinear trend, meaning that Newton's law of viscosity cannot be applied (Zhu et al., 2017; Gu et al., 2020). Generally, the most common fluids in engineering such as pseudoplastic fluids and dilatant fluids show shear-thinning and shear-thickening characteristics, respectively, and the most widely applied fluid model is the power law model (Zhang et al., 2016) that is suitable within a medium range of shear rate (Faltas and Saad, 2005). The buckling model (Wang et al., 2007) describes the effect of temperature on the viscosity of non-Newtonian fluids. The Prandtl-Eyring model (Hussain et al., 2019) was established for viscoelastic fluid and the description of zero shear viscosity. The micropolar fluid model (Eringen, 1966; Su, 2016) with asymmetric stress tensors can explain the complex flow composed of dipole elements. Other developed models are the Bingham model and the Herschel-Bulkley model (Pranesh, 2003; Huang and Wu, 2014), while the micropolar fluid model (Eringen, 1966) proposed by Eringen more directly reflects the non-Newtonian characteristics.

Several studies have presented the Hele-Shaw flow of micropolar fluids and its typical solutions, and these mean-

*Corresponding author.
E-mail address: weiyaook@sina.com (W. Zhu).

Yandy Scientific Press

2207-9963
Received November 27, 2021; revised December 6, 2021; accepted December 7, 2021; available online December 10, 2021.

ingful works provided some guidance for subsequent studies (Prakash and Sinha, 1975; Qiu, 1990; Aydin and Pop, 2005). However, the micropolar fluid involved in the above work is still assumed to satisfy the viscosity properties of a Newtonian fluid, leading to the neglect of the additional viscosity effect of micropolar fluid particles due to their own rotation in the resulting solution. In addition, the radial seepage of micropolar fluids in the formation has not been studied. Herein, in order to remedy these deficiencies, the Hele-Shaw flow equation for micropolar fluids was re-derived based on the classical micropolar theory. The obtained flow equation was solved by using the characteristic solution method of linear ordinary differential equation, while the micropolar effect was taken into account to reflect the increase of viscosity due to the rotation of fluid particles in the flow solution. Subsequently, a new form of analytical solution of the flow equation was obtained. On the basis of the obtained flow solutions, combined with the equation of continuity, equation of state, and equation of motion, a mathematical model of unsteady plane radial flow of a micropolar fluid in porous media was developed and solved. Actual field data from the Songliao Basin were selected for model reliability validation, and the effects of the ratio of rotational viscous force to Newtonian viscous force and the characteristic length of the micropolar element material on the pressure distribution, IPR curve, and percolation velocity were analyzed.

The micropolar fluid model can be employed to describe the migration of various fluids, such as the flow of blood (Roy and Beg, 2021), crystals (Lhuillier and Rey, 2004) and suspensions (Wang and Liu, 2005), showing broad suitability in the fields of lubrication, oil exploration, combustion products, environmental pollution reduction, drilling, etc (Fatunmbi and Salawu, 2020). This model is of great value for the study of micropolar fluid flow in porous media, both to provide theoretical guidance and to enhance practical engineering applications, such as in oil drilling, exploration and development, petrochemicals, and so on.

2. Theory and model

2.1 Hele-Shaw flow equation and solution for micropolar fluid

While it occurs within the narrow slit between two parallel glass plates (Kondic et al., 1996), as shown in Fig. 1, the Hele-Shaw flow is dominated by viscosity and features negligible inertia.

Under the assumptions of low velocity, unsteady state and insignificant gravity, the field equation in vector form (Murthy and Srinivas, 2013; Pramod et al., 2018) can be written as:

$$\begin{cases} \dfrac{\partial \rho}{\partial t}+\nabla(\rho\vec{v})=0 \\ -\nabla\Pi+(\lambda_v+2\mu_v+d_v)\nabla\nabla\vec{v}-(\mu_v+d_v)\nabla\times\nabla\times\vec{v} \\ +d_v\nabla\times\vec{w}+\rho\left(\vec{f}-\dot{v}\right)=0 \\ (\alpha_v+\beta_v+\gamma_v)\nabla\nabla\vec{w}-\gamma_v\nabla\times\nabla\times\vec{w}+d_v\nabla\times\vec{v} \\ -2d_v\vec{w}+\rho\left(\vec{L}-\dot{\sigma}\right)=0 \end{cases} \tag{1}$$

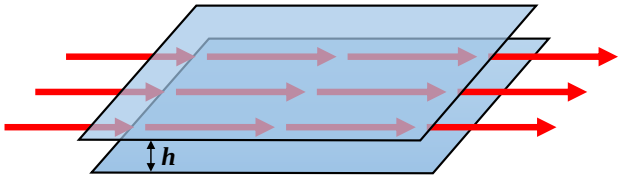

Fig. 1. Hele-Shaw flow model.

When neglecting the higher-order terms, body forces and couples in Eq. (1), then $\dot{v}=0$, $\vec{f}=0$, $\vec{L}=0$, $\sigma=0$. Subsequently, the simplified form of Eq. (1) is obtained as follows by replacing Π with pressure p:

$$\begin{cases} \dfrac{\partial \rho}{\partial t}+\nabla(\rho\vec{v})=0 \\ -\nabla p+(\lambda_v+2\mu_v+d_v)\nabla\nabla\vec{v}-(\mu_v+d_v)\nabla\times\nabla\times\vec{v} \\ +d_v\nabla\times\vec{w}=0 \\ (\alpha_v+\beta_v+\gamma_v)\nabla\nabla\vec{w}-\gamma_v\nabla\times\nabla\times\vec{w}+d_v\nabla\times\vec{v} \\ -2d_v\vec{w}=0 \end{cases} \tag{2}$$

or a further simplification can be expressed as

$$\begin{cases} \dfrac{\partial \rho}{\partial t}+\nabla(\rho\vec{v})=0 \\ -(\mu_v+d_v)\nabla\times\nabla\times\vec{v}+d_v\nabla\times\vec{w}-\nabla p=0 \\ -\gamma_v\nabla\times\nabla\times\vec{w}+d_v\nabla\times\vec{v}-2d_v\vec{w}=0 \end{cases} \tag{3}$$

where ρ represents the mass density, $\vec{v}$ represents the velocity vector, $\vec{w}$ represents the angular velocity vector, $\vec{f}$ represents the body force of unit mass, $\vec{L}$ represents the body couple, λ_v and μ_v represent the characteristic coefficients of classical fluid mechanics, and d_v, α_v, β_v, and γ_v are the new viscosity coefficients of micropolar fluid.

Considering the slit flow mentioned above, the height of the slit in the y direction is small. It can be assumed that the velocity and angular velocity of the micropolar fluid have the following form:

$$\begin{cases} \vec{v}=(u_1,u_2,u_3) \\ \vec{w}=(w_1,0,w_3) \end{cases} \tag{4}$$

Subsequently, Eq. (3) can be written as

$$\begin{cases} (\mu_v+d_v)\dfrac{\partial^2 u_1}{\partial y^2}+d_v\dfrac{\partial w_3}{\partial y}-\dfrac{\partial p}{\partial x}=0 \\ (\mu_v+d_v)\dfrac{\partial^2 u_3}{\partial y^2}-d_v\dfrac{\partial w_1}{\partial y}-\dfrac{\partial p}{\partial z}=0 \\ \gamma_v\dfrac{\partial^2 w_1}{\partial y^2}+d_v\dfrac{\partial u_3}{\partial y}-2d_v w_1=0 \\ \gamma_v\dfrac{\partial^2 w_3}{\partial y^2}-d_v\dfrac{\partial u_1}{\partial y}-2d_v w_3=0 \\ \dfrac{\partial p}{\partial y}=0 \\ \dfrac{\partial p}{\partial t}+\nabla(\rho\vec{v})=0 \end{cases} \tag{5}$$

The relevant boundary conditions are as follows:

$$\begin{cases} y=0: u_1=u_2=u_3=0, w_1=w_3=0 \\ y=h: u_1=u_2=u_3=0, w_1=w_3=0 \end{cases} \tag{6}$$

As a result of the independence of p and y, the first and fourth equations in Eq. (5) can be regarded as two ordinary differential equations (ODEs) that are satisfied by variables u_1 and w_3. Similarly, the second and third equations in Eq. (5) are ODEs for variables u_3 and w_1. Combined with the boundary conditions, a group of solutions can be derived as

$$\begin{cases} u_1 = -\dfrac{1}{2\mu_v+d_v}\dfrac{\partial p}{\partial x} \\ \quad \times\left[\left(hy-y^2\right)+\dfrac{N^2}{m}\dfrac{\mathrm{ch}(my)h-\mathrm{ch}(mh)y+(y-h)}{\mathrm{sh}(mh)}\right] \\ u_3 = -\dfrac{1}{2\mu_v+d_v}\dfrac{\partial p}{\partial z} \\ \quad \times\left[\left(hy-y^2\right)+\dfrac{N^2}{m}\dfrac{\mathrm{ch}(my)h-\mathrm{ch}(mh)y+(y-h)}{\mathrm{sh}(mh)}\right] \\ w_1 = -\dfrac{1}{2\mu_v+d_v}\dfrac{\partial p}{\partial z}\left[\dfrac{\mathrm{sh}(my)h}{\mathrm{sh}(mh)}-y\right] \\ w_3 = \dfrac{1}{2\mu_v+d_v}\dfrac{\partial p}{\partial x}\left[\dfrac{\mathrm{sh}(my)h}{\mathrm{sh}(mh)}-y\right] \end{cases} \tag{7}$$

In Eq. (7), $N=\left[d_v/\left(\mu_v+d_v\right)\right]^{0.5}$ and $m=\left\{\left(d_v^2+2\mu_v d_v\right)/\left[\gamma_v\left(\mu_v+d_v\right)\right]\right\}^{0.5}$.

The flow rate of unit width is expressed as:

$$\begin{cases} q_x=\displaystyle\int_0^h u_1\mathrm{d}y \\ \quad =-\dfrac{1}{2\mu_v+d_v}\dfrac{\partial p}{\partial x}\dfrac{h^3}{6}\left[1+6\bar{l}^2\left(1-\dfrac{\frac{N}{\bar{l}}\mathrm{ch}\frac{N}{\bar{l}}+\frac{N}{\bar{l}}}{2\mathrm{sh}\frac{N}{\bar{l}}}\right)\right] \\ q_z=\displaystyle\int_0^h u_3\mathrm{d}y \\ \quad =-\dfrac{1}{2\mu_v+d_v}\dfrac{\partial p}{\partial z}\dfrac{h^3}{6}\left[1+6\bar{l}^2\left(1-\dfrac{\frac{N}{\bar{l}}\mathrm{ch}\frac{N}{\bar{l}}+\frac{N}{\bar{l}}}{2\mathrm{sh}\frac{N}{\bar{l}}}\right)\right] \end{cases} \tag{8}$$

In the above equation, $l=N/m=\left[\gamma_v/\left(2\mu_v+d_v\right)\right]^{0.5}$. When $\bar{l}=l/h$, $\vec{q}=(q_x,q_z)$, and

$$\begin{aligned} \vec{q} &= -\frac{h^3}{6\left(2\mu_v+d_v\right)}\left[1+6\bar{l}^2\left(1-\frac{\frac{N}{\bar{l}}\mathrm{ch}\frac{N}{\bar{l}}+\frac{N}{\bar{l}}}{2\mathrm{sh}\frac{N}{\bar{l}}}\right)\right]\nabla p \\ &= -\frac{k}{\mu_v+\frac{d_v}{2}}\nabla p \end{aligned} \tag{9}$$

then the available the permeability of micropolar fluid will be

$$k=\frac{h^3}{12}\left[1+6\bar{l}^2\left(1-\frac{\frac{N}{\bar{l}}\mathrm{ch}\frac{N}{\bar{l}}+\frac{N}{\bar{l}}}{2\mathrm{sh}\frac{N}{\bar{l}}}\right)\right] \tag{10}$$

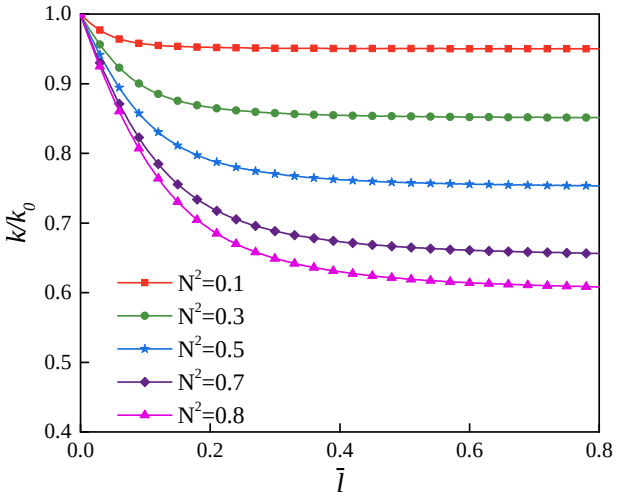

Fig. 2. Influence of micropolar fluid characteristics on the permeability change.

Eqs. (8)-(10) indicate a significant relation between the permeability and characteristic parameters of micropolar fluid. Compared with a Newtonian fluid, the appearance of dimensionless characteristic parameters N and $\bar{l}$ is the most conspicuous difference. From the physical meaning of N^2 and $\bar{l}$, Eq. (8) degenerates to an expression of Newtonian fluid when $N^2=0$. Eq. (9) reflects Darcy's law of a micropolar fluid. Since $k_0=h^3/12$ is the permeability of a Newtonian fluid (Biao et al., 2011), Eq. (10) can be rewritten as

$$k_{mr}=\frac{k}{k_0}=1+6\bar{l}^2\left(1-\frac{\frac{N}{\bar{l}}\mathrm{ch}\frac{N}{\bar{l}}+\frac{N}{\bar{l}}}{2\mathrm{sh}\frac{N}{\bar{l}}}\right) \tag{11}$$

$$k=k_0k_{mr} \tag{12}$$

where k_{mr} is the relative permeability of micropolar fluid.

Fig. 2 illustrates the effect of micropolar parameters N^2 and $\bar{l}$ on the apparent permeability k_m on the basis of the calculation performed through Eq. (10). With the increase in N^2, k_{mr} shows a decreasing trend when $\bar{l}$ is constant, while the reduction of k_m is proportional to N^2. For a fixed N^2, k_{mr} decreases as $\bar{l}$ increases. When $\bar{l}$ is less than 0.4, the change of k_m along with $\bar{l}$ is significant than that when $\bar{l}$ is larger than 0.4, in which case k_{mr} can be regarded as a constant.

2.2 Unsteady mathematical model and relevant solution of micropolar fluid

2.2.1 Mathematical model of micropolar fluid flow in porous media

Although it is difficult to study flow in porous media that has a complex structure, it can be approximated by the Hele-Shaw flow based on similarity. According to previous analysis and experience, the porous media is assumed to be constructed by countless pores with a size of h that satisfies a distribution function $\Phi(h)$, and the apparent permeability of micropolar fluid can be logically given as

$$k_m = \int_{h_{\min}}^{h_{\max}} k(h)\Phi(h)\mathrm{d}h = \int_{h_{\min}}^{h_{\max}} \frac{h^3}{12}\left[1+6\frac{l^2}{h^2}-3\frac{ml^2}{h^2}\frac{\mathrm{ch}(mh)+1}{\mathrm{sh}(mh)}\right]\Phi(h)\mathrm{d}h = k_0 + \int_{h_{\min}}^{h_{\max}} \frac{hl^2}{2}\left[1-\frac{mh\,(\mathrm{ch}(mh)+1)}{2\mathrm{sh}(mh)}\right]\Phi(h)\mathrm{d}h \quad (13)$$

Eq. (13) presents the dependence of k_m on pore structure and micropolar fluid characteristics.

For compressible fluids,

$$\rho = \rho_0\left[1+C_\rho\,(p-p_0)\right] \quad (14)$$

The porosity of a compressible formation is

$$\phi = \phi_0\left[1+C_\phi\,(p-p_0)\right] \quad (15)$$

The motion equation of a micropolar fluid is expressed as:

$$\vec{v} = -\frac{k_m}{\mu_v+\frac{d_v}{2}}\nabla p \quad (16)$$

The mass conservation equation is:

$$\frac{\partial(\rho\phi)}{\partial t} = -\mathrm{div}(\rho\vec{v}) \quad (17)$$

Substituting Eqs. (14)-(16) into Eq. (17) yields the following equation:

$$\frac{\partial p}{\partial t} = \frac{1}{\phi C_t}\mathrm{div}\left(\frac{k_m}{\mu_v+\frac{d_v}{2}}\nabla p\right) \quad (18)$$

Based on the linear theory of micropolar fluid introduced above, and that Eq. (1) is a field equation with constants λ_v, μ_v, d_v, α_v, β_v, and γ_v, Eq. (18) can be written as:

$$\frac{\partial p}{\partial t} = \frac{k_0 k_{mr}}{\phi C_t\left(\mu_v+\frac{d_v}{2}\right)}\nabla^2 p = \frac{k_0}{\phi C_t\mu_v}\frac{k_{mr}}{\left(1+\frac{d_v}{2\mu_v}\right)}\nabla^2 p = d_0 k_{dr}\nabla^2 p \quad (19)$$

where $d_0 = k_0/(\phi C_t\mu_v)$, $k_{dr} = k_{mr}/[1+d_v/(2\mu_v)]$.

Eq. (19) reflects the feature of the propagation of micropolar fluid pressure, which is obviously related to the characteristics of micropolar fluid.

2.2.2 Solution for micropolar fluid flow in an infinite formation

Assuming that the formation that has H thickness and plate shape is homogeneous and is enclosed by a supply boundary, and a penetrated well of radius r_w is located at the center of the formation, the solution of the model can be obtained as

$$p_i - p_{(r,t)} = \frac{Q\left(\mu_v+\frac{d_v}{2}\right)}{2\pi k_m H}\left[-\mathrm{Ei}\left(-\frac{r^2}{4d_0k_{dr}t}\right)\right] \quad (20)$$

where Ei represents a power integral, p_i represents the original formation pressure, $p_{(r,t)}$ represents the pressure at distance r and time t, d_0 represents the pressure transmitting coefficient, t represents the production time of the well, Q represents the well production, μ_v represents the viscosity of Newtonian fluid, k_m represents the micropolar fluid permeability, H represents the formation thickness, C_t is comprehensive elastic compression coefficient, r represents the distance from the center, and d_v represents the viscosity coefficient of micropolar fluid. According to Eq. (20), viscosity d_v has a significant impact on pressure propagation.

3. Results and discussion

3.1 A case analysis

The Songliao Basin is located in Northeast China, extending across Heilongjiang, Jilin, Liaohe and Inner Mongolia (Yang et al., 2021). It is a large Mesozoic continental petroliferous basin developed on the hercynian fold basement with a fault-depression dual geological structure (Deng et al., 2021). It covers an area of about 26×10^4 km^2 and has experienced three evolutionary stages: early Cretaceous extensional fault depression, Middle Cretaceous depression, and middle and late Cretaceous regression (Yi et al., 2021). Lithologic stratigraphic traps are controlled by the lacustrine delta sedimentary environment and located near the transition zone between lacustrine facies (Gao et al., 2021). The large and shallow lacustrine delta systems formulated in the Songliao Basin provide favorable conditions for the development of lithologic stratigraphic traps. The oil and gas resources are rich, and the geological petroleum resources amount to around 15 billion tons (Sun et al., 2007; Gao et al., 2018; Zhang et al., 2021).

In order to verify the accuracy of the model, this paper carries out evaluation through practical problems. The historical fitting was carried out based on an oil production well in the Songliao Basin. The production cycle of the well was 400 days in total, and the development mode was infinite formation variable production and pressure development. The production history curve is shown in Fig. 3, and the reservoir and production parameters used in the calculation are presented in Table 1. All of the basic parameters were input into the model established in this paper, and the yield prediction results were compared with the actual production data. The coincidence rate of the daily fluid production curve was 94.21%, which shows good matching with the field data, verifying the accuracy of the proposed mathematical model.

3.2 Characteristics of micropolar fluid flow in formation

3.2.1 Pressure distribution

Fig. 4 and Fig. 5 exhibit the difference between the pressure distribution of micropolar fluid and Newtonian fluid.

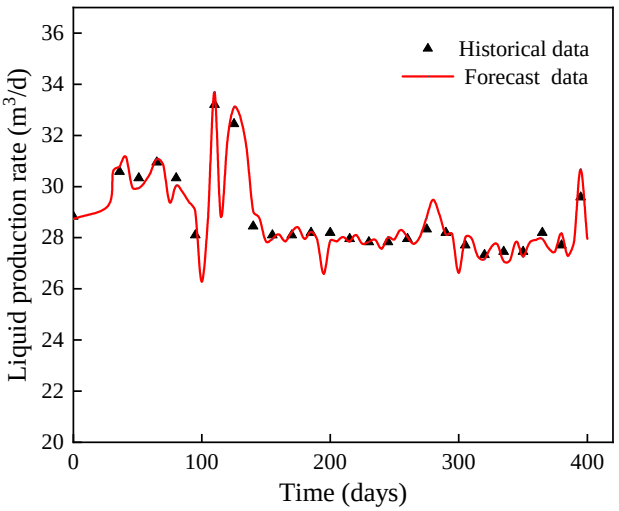

Fig. 3. Comparison of the calculated results and the actual production rate.

Table 1. Input parameters for model verification.

Parameter	Value
Initial formation pressure P_i (MPa)	24
Porosity ϕ	0.26
Reservoir thickness H (m)	10
Newtonian fluid permeability k_0 (m^2)	2×10^{-13}
Total compressibility C_t (Pa^{-1})	1.29×10^{-9}
Viscosity μ_v (Pa·s)	0.01

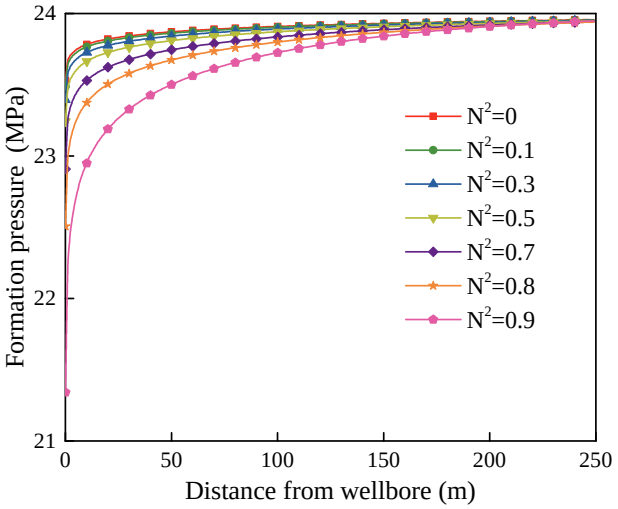

Fig. 4. Characteristic pressure variation for different values of micropolar parameter N^2.

At the same flow rate, the non-Newtonian property is enhanced with the increase of N^2 and $\bar{l}$, thus the pressure consumption of micropolar fluid is much larger than that of Newtonian fluid. A stronger micropolar property indicates a larger pressure drop. The influence of micropolar parameter N^2 on pressure distribution is shown in Fig. 4. When $N^2 < 0.3$, the pressure

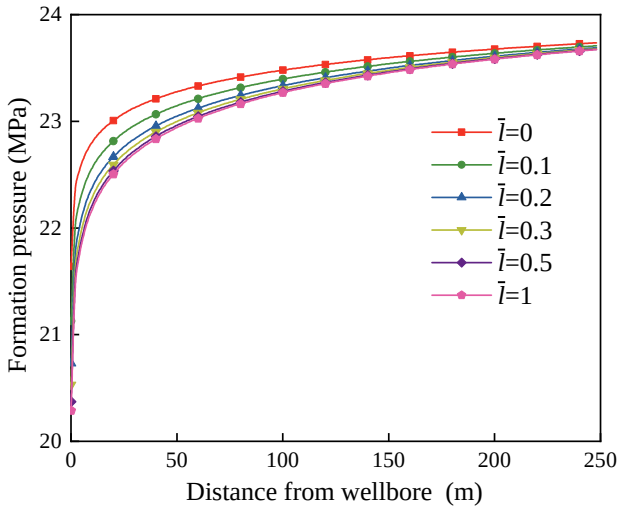

Fig. 5. Characteristic pressure variation for different values of micropolar parameter $\bar{l}$.

curves are almost identical, suggesting that the effect of parameter N^2 can be neglected. When $N^2 > 0.3$, the difference between micropolar fluid and Newtonian fluid becomes significantly larger, which becomes more apparent with the value of N^2 increasing. The pressure drop is in inverse relationship with parameter $\bar{l}$ when $\bar{l} < 0.5$, meaning that the pressure-drop curves show distinct differences. If $\bar{l}$ exceeds 0.5, the pressure-drop curves are nearly overlapped, which reflects the decreasing impact of $\bar{l}$ on pressure. The distinguishing feature of micropolar fluid is the larger apparent viscosity and resulting increased flow resistance, which leads to greater energy consumption, a wider pressure drop range, and lower production.

3.2.2 Velocity distribution

The influence of micropolar parameters on the velocity curve is shown in Fig. 6 and Fig. 7. Under a certain pressure gradient, the flow velocity gradually decreases with the increase of micropolar parameters N^2 and $\bar{l}$, and parameter N^2 has a greater influence on velocity. As can be seen from Fig. 6, the velocity curves change obviously with parameter N^2 that is less than 0.7. When $N^2 > 0.7$, the velocity is barely affected by parameter N^2, and the effect of N^2 decreases when N^2 increases. It can be observed from Fig. 7 that velocity obviously varies with $\bar{l}$ when $\bar{l} < 0.5$, whereas it is not significantly related to $\bar{l}$ when $\bar{l} > 0.5$. The cause of the above phenomenon lies in the non-Newtonian property of fluid that increases with micropolar parameters, resulting in larger flow resistance and making the energy supply minimally effective.

3.2.3 Effect on inflow performance relationship curve

Fig. 8 and Fig. 9 show the influence of micropolar parameters on the Inflow Performance Relationship (IPR) curve, in which the negative reciprocal of slope represents the oil production index that reflects the oil feeding capacity of wells (Wu et al., 2018). The oil production index shows a decreasing trend when the enlargement of parameters N^2 and $\bar{l}$ appears. As can be seen from Fig. 8, the overlap of the IPR curves is

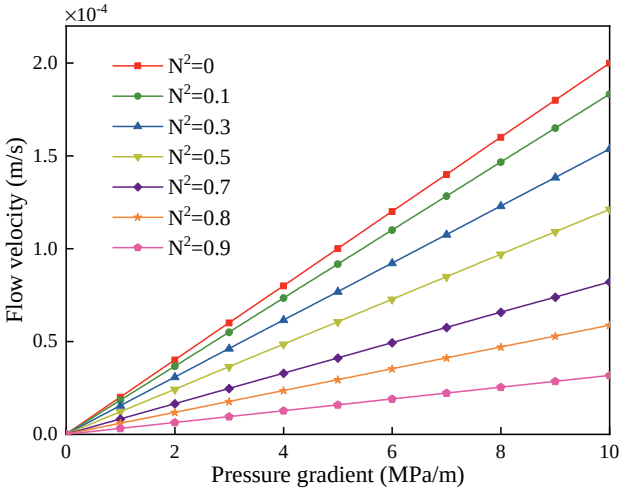

Fig. 6. Flow velocity curves for different values of micropolar parameter N^2.

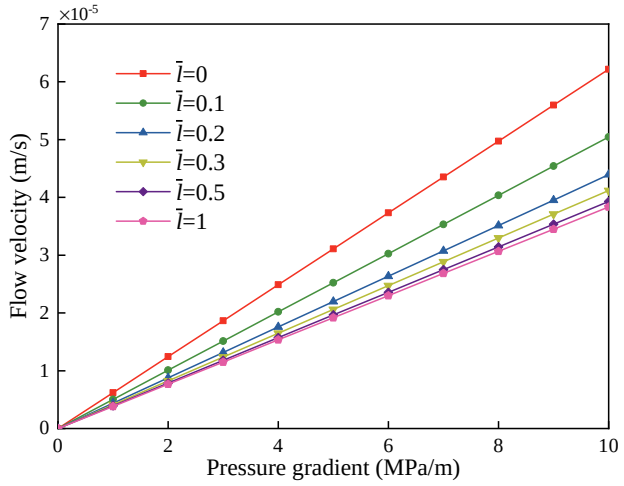

Fig. 7. Flow velocity curves for different values of micropolar parameter $\bar{l}$.

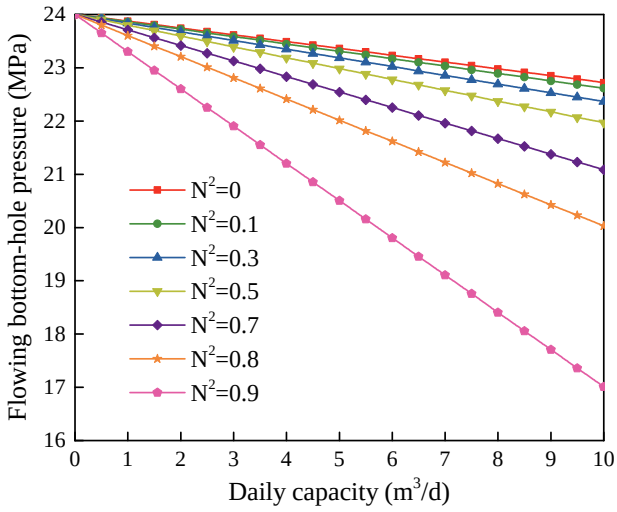

Fig. 8. IPR curves for different values of micropolar parameter N^2.

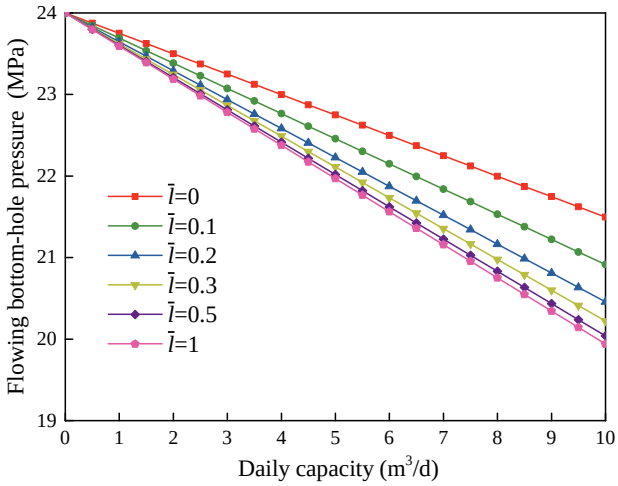

Fig. 9. IPR curves for different values of micropolar parameter $\bar{l}$.

driven little by the effect of parameter N^2 that is less than 0.3. However, increasing the production rate creates a rapidly reduced flowing bottomhole pressure, which becomes dramatic when $N^2 > 0.3$. Fig. 9 indicates that a value of $\bar{l}$ of less than 0.5 has obvious influence on the IPR curve, while that larger than 0.5 does not. As the micropolar parameter increases, the fluidity of formation fluid becomes worse.

4. Conclusions

(1) In this paper, a mathematical model of micropolar fluid Hele-Shaw flow is established, and its analytical solution is further obtained based on field theory. The micropolar parameters N^2 and $\bar{l}$ that have a significant impact on apparent permeability are the differences between the solutions of micropolar fluid and Newtonian fluid.

(2) Based on the newly established unsteady mathematical model of micropolar fluid radial flow in an infinite formation, the analytical solution of pressure distribution features dependence on the characteristics of micropolar fluid, especially viscosity d_v, which deviates from that of Newtonian fluid. As a result, the larger apparent viscosity of micropolar fluid causes a larger flow resistance that raises the pressure consumption.

(3) The calculation reveals that the parameter N^2 with a value exceeding 0.3 or $\bar{l}$ that is less than 0.5 significantly affects pressure distribution and the oil production index, and this effect is proportional to N^2. The increases in N^2 and $\bar{l}$ are related to the enhancement of non-Newtonian property of micropolar fluid, which leads to reduced well production.

Acknowledgement

This work was financially supported by the National Natural Science Foundation of China (Grant No. 51974013). Additional thanks are given to Hongyang Chu, Yubao Gao, Wengang Bu and Qipeng Ma for contributing to the text and graphics work of this article.

Nomenclature

C_t = Total compressibility, Pa^{-1}
$\vec{f}$ = Body force per unit mass, N/kg

h = Plate flow channel height, m
H = Formation thickness, m
d_0 = Pressure transmitting coefficient, $m^2 \cdot Pa/(Pa \cdot s)$
k_{mr} = Relative permeability of micropolar fluid
k = Available the permeability of micropolar fluid, m^2
k_0 = Newtonian fluid permeability, m^2
k_m = Micropolar fluid permeability, m^2
$\vec{L}$ = Body moments per unit mass
p = Fluid pressure, Pa
p_i = Original formation pressure, Pa
$p_{(r,t)}$ = Pressure at distance r and time t, Pa
Q = Production rate, m^3/s
r = Supply radius, m
t = Production time, s
$\vec{v}$ = Velocity vector, m/s
$\dot{v}$ = Inertial acceleration, m/s^2
$\vec{w}$ = Micro-rotation velocity vector, rad/s
d_v, α_v, β_v, and γ_v = Viscosity coefficient of the micropolar fluid
λ_v and μ_v = Viscosity of the Newtonian fluid, $Pa \cdot s$
$\prod$ = Thermodynamic pressure, Pa
ρ = Fluid density, kg/m^3
$\dot{\sigma}$ = Inertial spin
ϕ = Porosity
ρ_0 = Fluid density at initial pressure, kg/m^3
C_ρ = Fluid compressibility, Pa^{-1}
p_0 = Initial pressure, Pa
ϕ_0 = Porosity at initial pressure
C_ϕ = Rock compressibility, Pa^{-1}

Conflict of interest

The author declares no competing interest.

References

Aydin, O., Pop, I. Natural convection from a discrete heater in enclosures filled with a micropolar fluid. International Journal of Engineering Science, 2005, 43(19-20): 1409-1418.

Biao, F., Liu, H., Zhang, S., et al. A numerical study of parameter influences on horizontal hydraulic fracture. Engineering Mechanics, 2011, 28: 228-235. (in Chinese)

Chang-Jian, C. W., Chen, C. K. Nonlinear dynamic analysis of a flexible rotor supported by micropolar fluid film journal bearings. International Journal of Engineering Science, 2006, 44: 1050-1070.

Chen, Z. M., Price, W. G. Decay estimates of linearized micropolar fluid flows in R3 space with applications to L3-strong solutions. International Journal of Engineering Science, 2006, 44(13-14): 859-873.

Deng, Q., Hu, M., Kane, O. I., et al. Syn-rift sedimentary evolution and hydrocarbon reservoir models in a graben rift sag, Songliao Basin, northeast China. Marine and Petroleum Geology, 2021, 132: 105245.

Ellahi, R., Rahman, S., Gulzar, M. M., et al. A mathematical study of non-Newtonian micropolar fluid in arterial blood flow through composite stenosis. Applied Mathematics and Information Sciences, 2014, 8(4): 1567-1573.

Eringen, A. C. Theory of micropolar fluids. Journal of Mathematics and Mechanics, 1966, 16(1): 1-18.

Faltas, M. S., Saad, E. I. Stokes flow with slip caused by the axisymmetric motion of a sphere bisected by a free surface bounding a semi-infinite micropolar fluid. International Journal of Engineering Science, 2005, 43(11-12): 953-976.

Fatunmbi, E., Salawu, S. Thermodynamic second law analysis of magneto-micropolar fluid flow past nonlinear porous media with non-uniform heat source. Propulsion and Power Research, 2020, 9(3): 281-288.

Gao, F., Song, Y., Li, Z., et al. Lithofacies and reservoir characteristics of the lower cretaceous continental shahezi shale in the changling fault depression of Songliao Basin, NE China. Marine and Petroleum Geology, 2018, 98: 401-421.

Gao, Y., Gao, Y., Ibarra, D. E., et al. Clay mineralogical evidence for mid-latitude terrestrial climate change from the latest cretaceous through the earliest paleogene in the Songliao Basin, NE China. Cretaceous Research, 2021, 124: 104827.

Gu, C., Qiu, R., Liu, S., et al. Shear thickening effects of drag-reducing nanofluids for low permeability reservoir. Advances in Geo-Energy Research, 2020, 4(3): 317-325.

Huang, R., Wu, H. A modified multiple relaxation time lattice Boltzmann model for convection-diffusion equation. Journal of Computational Physics, 2014, 274: 50-63. (in Chinese)

Hussain, A., Malik, M., Awais, M., et al. Computational and physical aspects of mhd prandtl-eyring fluid flow analysis over a stretching sheet. Neural Computing and Applications, 2019, 31(1): 425-433.

Kondic, L., Palffy, M. P., Shelley, M. J. Models of non-Newtonian Hele-Shaw flow. Physical Review E, 1996, 54(5): 4536-4539.

Lhuillier, D., Rey, A. D. Nematic liquid crystals and ordered micropolar fluids. Journal of non-Newtonian Fluid Mechanics, 2004, 120(1-3): 169-174.

Lok, Y. Y., Pop, I., Chamkha, A. J. Non-orthogonal stagnation-point flow of a micropolar fluid. International Journal of Engineering Science, 2007, 45(1): 173-184.

Masuda, Y., Tang, K. C., Miyazawa, M., et al. 1D simulation of polymer flooding including the viscoelastic effect of polymer solution. SPE Reservoir Engineering, 1992, 7(2): 247-252.

Mohamadian, N., Ghorbani, H., Wood, D. A., et al. Rheological and filtration characteristics of drilling fluids enhanced by nanoparticles with selected additives: An experimental study. Advances in Geo-Energy Research, 2018, 2(3): 228-236.

Murthy, J., Srinivas, J. Second law analysis for poiseuille flow of immiscible micropolar fluids in a channel. International Journal of Heat and Mass Transfer, 2013, 65: 254-264.

Nabwey, H. A., Mahdy, A. Numerical approach of micropolar dust-particles natural convection fluid flow due to a

permeable cone with nonlinear temperature. Alexandria Engineering Journal, 2021, 60(1): 1739-1749.

Prakash, J., Sinha, P. Lubrication theory for micropolar fluids and its application to a journal bearing. International Journal of Engineering Science, 1975, 13(3): 217-232.

Pramod, K. Y., Sneha, J., Taimoor, A., et al. Influence of a magnetic field on the flow of a micropolar fluid sandwiched between two newtonian fluid layers through a porous medium. European Physical Journal Plus, 2018, 133(7): 247-260.

Pranesh, S. Effects of suction-injection-combination (SIC) on the onset of rayleigh-benard magnetoconvection in a micropolar fluid. International Journal of Engineering Science, 2003, 41(15): 1741-1766.

Qiu, Z. Hele-shaw flow for micropolar fluids. Journal of Fudan University (Natural Science), 1990, 29(2): 129-135. (in Chinese)

Roy, A. K., Beg, O. A. Mathematical modelling of unsteady solute dispersion in two-fluid (micropolar-newtonian) blood flow with bulk reaction. International Communications in Heat and Mass Transfer, 2021, 122: 105169.

Siddheshwar, P. G., Manjunath, S. Unsteady convective diffusion with heterogeneous chemical reaction in a plane-poiseuille flow of a micropolar fluid. International Journal of Engineering Science, 2000, 38(7): 765-783.

Su, J. Incompressible limit of a compressible micropolar fluid model with general initial data. Nonlinear Analysis, 2016, 132: 1-24.

Sun, S., Shu, L., Zeng, Y., et al. Porosity-permeability and textural heterogeneity of reservoir sandstones from the lower cretaceous putaohua member of yaojia formation, weixing oilfield, Songliao Basin, Northeast China. Marine and Petroleum Geology, 2007, 24(2): 109-127.

Wang, W., Liu, K., Jiao, M. Thermal and non-Newtonian analysis on mixed liquid-solid lubrication. Tribology International, 2007, 40(7): 1067-1074.

Wang, X. L., Liu, W. Derivation and application of energy equation for the lubrication with micropolar fluids. Journal of Beijing Institute of Technology, 2005, 25: 380-383. (in Chinese)

Wu, C., Liu, X., Liu, Y. Method of specific productivity index prediction of huanghekou sag and its application. Fault Block Oil and Gas Field, 2018, 25(2): 218-221. (in Chinese)

Yadav, P. K., Kumar, A. An inclined magnetic field effect on entropy production of non-miscible newtonian and micropolar fluid in a rectangular conduit. International Communications in Heat and Mass Transfer, 2021, 124: 105266.

Yang, X., Wang, H., Li, Z., et al. Tectonic-sedimentary evolution of a continental rift basin: A case study of the early cretaceous changling and lishu fault depressions, southern Songliao Basin, China. Marine and Petroleum Geology, 2021, 128: 105068.

Yi, S., Li, M., Xu, S., et al. Accumulation condition and model of buried hill in the central uplift, Songliao Basin, China. Journal of Natural Gas Geoscience, 2021, 6(3): 121-135.

Zhang, H., Xu, T., Zhang, X., et al. Study on local resistance of non-Newtonian power law fluid in elbow pipes. Journal of Thermal Science, 2016, 25(3): 287-291.

Zhang, L., Bao, Z., Dou, L., et al. Diagenetic alterations related to sedimentary architecture of deltaic distributary channels in red beds of the cretaceous yaojia formation, songliao basin. Journal of Petroleum Science and Engineering, 2021, 203: 108564.

Zhu, L., Yuan, Z., Xu, Y., et al. Shear thinning property analysis of non-Newtonian fluid mold flux. Steelmaking, 2017, 33(3): 25-30. (in Chinese)